JUN 23 1982

NAS 1.26:3562

NASA Contractor Report 3562

ORIGINAL

COMPLETED
61

Analysis of the Scramjet Inlet Flow Field Using Two-Dimensional Navier-Stokes Equations

Ajay Kumar and S. N. Tiwari

CONTRACT NAS1-15930
JUNE 1982

NASA

NASA Contractor Report 3562

Analysis of the Scramjet Inlet Flow Field Using Two-Dimensional Navier-Stokes Equations

Ajay Kumar and S. N. Tiwari
Old Dominion University
Norfolk, Virginia

Prepared for
Langley Research Center
under Contract NAS1-15930

NASA
National Aeronautics
and Space Administration

**Scientific and Technical
Information Office**

1982

I BEST DOCUMENT AVAILABLE

BEST DOCUMENT AVAILABLE

Foreword

This report covers the final work completed on the research project "Scramjet Inlet Analysis." The work was supported by the NASA/Langley Research Center (Hypersonic Propulsion Branch of the High-speed Aerodynamics Division) through research contract NAS1-15930. The contract was monitored by Dr. Harry L. Beach, Jr. of the High-Speed Aerodynamics Division.

SUMMARY

A computer code has been developed to solve the full two-dimensional Navier-Stokes equations in a scramjet inlet. The analysis uses a numerical coordinate transformation which generates a set of boundary-fitted curvilinear coordinates. The explicit finite-difference algorithm of MacCormack is used to solve the governing equations. A two-layer eddy viscosity model is used for the turbulent flow. The code can analyze both inviscid and viscous flows with multiple struts in the flow field. Detailed results are presented for two model problems and two scramjet inlets with one and two struts. The application of the two-dimensional analysis in the preliminary design of the actual scramjet inlet is briefly discussed.

INTRODUCTION

NASA/Langley Research Center (LaRC) is currently engaged in developing an air-frame-integrated, hydrogen-fueled, supersonic combustion, ramjet engine (scramjet) for hypersonic speeds (refs. 1 and 2). Vehicle-propulsion system integration provides the use of the vehicle forebody to precompress the engine airflow before it enters the inlet and the use of the vehicle afterbody for additional expansion of the nozzle exhaust gas. Figure 1 shows the basic engine concept. It is seen that the entire under surface of the vehicle is part of the propulsion system. At high Mach numbers, the need for integration arises because almost all of the airflow between the vehicle and its bow shock is required by the engine for good performance. This suggests an inlet capture area with an annular shape. By splitting the

BEST DOCUMENT AVAILABLE

annular area into smaller rectangular modules, the primary engine becomes a system of identical units of size and shape appropriate for test in ground facilities. One such rectangular module is shown in figure 2 with a cross-sectional view at the bottom of the figure. The module has a fixed-geometry inlet with wedge-shaped sidewalls. Sweep of these sidewalls, in combination with a recess in the cowl, allows spillage to occur efficiently with fixed geometry of the inlet. Inlet compression is completed by three wedge-shaped struts located at the minimum-area section.

Considerable aerodynamic testing over a period of years has resulted in an inlet design which performs well over a wide Mach number range (refs. 3 and 4). The basic design features of this inlet are described in reference 3. A problem that has been discovered in the experimental work is an interaction between the combustion-induced disturbances and the inlet flow; this has resulted in either increased spillage from the inlet or complete engine unstart. Although this interaction problem is being investigated in further inlet and engine tests, it has not yet been addressed analytically. With the availability of high-speed computers, it is now feasible to analytically study the flow in a scramjet inlet. This will not only help in analyzing the problems observed experimentally but will also allow a parametric study in the inlet design with a substantial reduction in cost and time.

The flow in the scramjet inlet is highly three-dimensional, possibly turbulent, and has complex shock-expansion wave interactions. It also involves strong shock-boundary layer interactions which may result in separated regions. To analyze such flows, it is necessary to use the full Navier-Stokes equations with proper turbulence modeling. The objective of this

BEST DOCUMENT AVAILABLE

work is to develop a numerical code to analyze the scramjet inlet flow field. A two-dimensional code has been developed initially to gain understanding of some features of the inlet flow.

The two-dimensional Navier-Stokes equations in conservative law form are used to describe the inlet flow. In order to facilitate the treatment of a general inlet geometry with embedded bodies, a numerical coordinate transformation is employed which generates a set of boundary-fitted curvilinear coordinates (ref. 5). It transforms the physical domain into a rectangular domain with uniform mesh spacing, and embedded bodies are transformed into slits. The transformation allows for concentrating mesh lines in regions of high gradients. The transformed governing equations are solved by an explicit, time asymptotic, finite-difference method due to MacCormack (ref. 6). This explicit method is highly efficient on the vector-processing CDC-Cyber-203 computer at NASA/LaRC for which the current code is written.

The code, in its present form, can analyze both inviscid and viscous (laminar and turbulent) flows with no-strut, one strut, or multiple struts in the flow field. In order to explore the potential of the code, several model problems have been solved. The results for two such problems are presented here. Detailed results for actual inlet geometries with one and two struts in the flow field are also presented. It is also indicated how this two-dimensional analysis can be used to estimate the flow spillage from an actual three-dimensional inlet of the type shown in figure 2. An extension of the code to three dimensions is currently underway.

BEST DOCUMENT AVAILABLE

LIST OF SYMBOLS

H	total enthalpy
h	static enthalpy
J	Jacobian determinant
M_1	Mach number at the face of the inlet
M_∞	free-stream Mach number
Pr	laminar Prandtl number
Pr_t	turbulent Prandtl number
p	pressure
p_1	pressure at the face of the inlet
q_x, q_y	components of heat flux in x, y system
k	gas constant
T	temperature
T_1	temperature at the face of the inlet
t	time
u, v	components of velocity in x, y system
$\bar{u}$, $\bar{v}$	transformed velocities defined in equation (3)
x, y	Cartesian coordinates
ζ, η	transformed coordinates
σ_x, σ_y, τ_{yx}	components of stress tensor in x, y system
ρ	density
μ	$\mu_\ell + \mu_t$
μ_ℓ	laminar viscosity
μ_t	turbulent viscosity
ω	sweep angle of the sidewall leading edge

BEST DOCUMENT AVAILABLE

ANALYSIS

Introduction

This section describes the coordinate transformation, governing equations, and the method of solution. Boundary and initial conditions are also discussed.

Coordinate Transformation

In order to facilitate the treatment of a general inlet geometry with embedded bodies, a numerical coordinate transformation is employed which generates a set of boundary-fitted curvilinear coordinates, $\zeta(x,y)$ and $\eta(x,y)$. It transforms the physical domain into a rectangular domain with uniform mesh spacings in the ζ and η directions. Embedded bodies are transformed into slits. As an example, figure 3(a) shows an inlet geometry with a strut EFGH sitting in the flow field. Figure 3(b) shows the inlet in the transformed plane. The outer boundary of the inlet, ABCD, is transformed to a rectangle A'B'C'D' and the strut EFGH is transformed to a slit E'G'. The upper surface of the strut is made coincident with one of the mesh lines and the lower surface of the strut is treated separately. The transformation allows for concentrating the mesh lines in regions of high gradients such as around the strut or near boundary surfaces.

The coordinates are obtained using the approach of Thompson et al. (ref. 5) in which $\zeta(x,y)$ and $\eta(x,y)$ are solutions of the following equations:

$$\nabla^2 \zeta = P(\zeta,\eta) \qquad (1) \text{ (cont'd)}$$

BEST DOCUMENT AVAILABLE

$$\nabla^2 \eta = Q(\zeta,\eta) \qquad (1)$$
(concl'd)

where ∇^2 is the Laplacian operator $\partial^2/\partial x^2 + \partial^2/\partial y^2$; $P(\zeta,\eta)$ and $Q(\zeta,\eta)$ are the source terms used to control the spacing of ζ = constant; and η = constant lines in the physical plane. In the present analysis, these terms are used in the form described in reference 5. The coordinates $\zeta(x,y)$ and $\eta(x,y)$ are subject to Dirichlet boundary conditions along boundaries AC and BD and Neumann boundary conditions along boundaries AB and CD. The Navier-Stokes equations are solved in the transformed plane, and the inlet flow field in the physical plane is obtained using the inverse transformation $x(\zeta,\eta)$ and $y(\zeta,\eta)$.

Governing Equations

Two-dimensional Navier-Stokes equations in fully conservative form are used to describe the inlet flow. The transformed equations can be written as:

$$\frac{\partial U}{\partial t} + \frac{\partial M}{\partial \zeta} = \frac{\partial N}{\partial \eta} = 0 \qquad (2)$$

where

$$U = j \begin{bmatrix} \rho \\ \rho u \\ \rho v \\ \rho H - p \end{bmatrix}$$

$$M = \begin{bmatrix} \rho\bar{u} \\ \rho u\bar{u} + y_\eta\, \sigma_x - x_\eta\, \tau_{yx} \\ \rho v\bar{u} + y_\eta\, \tau_{xy} - x_\eta\, \sigma_y \\ \rho H\bar{u} - p\bar{u} + y_\eta\, (u\sigma_x + q_x) - x_\eta\, (v\sigma_y + q_y) + \tau_{yx}\, (vy_\eta - ux_\eta) \end{bmatrix}$$

and

BEST DOCUMENT AVAILABLE

$$N = \begin{bmatrix} \rho\bar{v} \\ \rho u\bar{v} - y_\zeta \sigma_x + x_\zeta \tau_{yx} \\ \rho v\bar{v} - y_\zeta \tau_{yx} - x_\zeta \sigma_y \\ \rho H\bar{v} - p\bar{v} - y_\zeta (u\sigma_x + q_x) + x_\zeta (v\sigma_y + q_y) + \tau_{yx} (-vy_\zeta - ux_\zeta) \end{bmatrix}$$

Here, x_ζ denotes $\partial x/\partial\zeta$, etc. and

$$\bar{u} = y_\eta u - x_\eta v$$

$$\bar{v} = -y_\zeta u + x_\zeta v$$

$$J = x_\zeta y_\eta - x_\eta y_\zeta \qquad (3)$$

The quantities σ_x, σ_y, and τ_{yx} are components of the stress tensor and are given by:

$$\sigma_x = p + \frac{2\mu}{3}\frac{\partial v}{\partial y} - \frac{4\mu}{3}\frac{\partial u}{\partial x}$$

$$\sigma_y = p + \frac{2\mu}{3}\frac{\partial u}{\partial x} - \frac{4\mu}{3}\frac{\partial v}{\partial y}$$

$$\tau_{yx} = -\mu\left(\frac{\partial u}{\partial y} + \frac{\partial v}{\partial x}\right) \qquad (4)$$

The components of heat flux, q_x and q_y, are given by:

$$q_x = -\left(\frac{\mu_\ell}{Pr} + \frac{\mu_t}{Pr_t}\right)\frac{\partial h}{\partial x} \qquad \begin{matrix}(5)\\(\text{cont'd})\end{matrix}$$

BEST DOCUMENT AVAILABLE

$$q_y = -\left(\frac{\mu_\ell}{Pr} + \frac{\mu_t}{Pr_t}\right)\frac{\partial h}{\partial y} \qquad (5) \text{ (concl'd)}$$

In order to complete the set of governing equations, equation of state $p = \rho RT$ is used, where R is the gas constant.

In equations (4), μ is the sum of laminar viscosity and turbulent viscosity. The laminar viscosity for air is calculated from Sutherland's law. The turbulent viscosity is calculated from an algebraic, two-layer eddy viscosity model due to Baldwin and Lomax (ref. 7). This model does not require the knowledge of the boundary- ayer thickness; instead, the model uses the vorticity at each point in the flow field to characterize the scale of turbulence. The model as such consists of an inner law and outer law. The inner law is applicable from the wall out to the location in the flow where the eddy viscosity given by the inner law is equal to that of the outer law. The outer law then is assumed applicable for the remainder of the flow. Details of the model are given in reference 7 along with the values of various constants used in the model.

Method of Solution

The governing equations are solved by a time-asymptotic, two-step, finite-difference method due to MacCormack (ref. 6). This explicit method has second-order accuracy in both space and time and is highly efficient on the CDC-Cyber-203 vector processing computer for which the current code is written. If a solution to equation (2) is known at some time $t = n\Delta t$, the solution at the next time step, $t = (n + 1)\Delta t$ can be obtained from

BEST DOCUMENT AVAILABLE

$$U^{n+1}_{i,j} = L(\Delta t)\, U^{n}_{i,j} \tag{6}$$

for each node point (i,j). The finite-difference operator L consists of a predictor step and a corrector step. Spatial derivatives in the predictor step are calculated by forward differences, while in the corrector step they are calculated by backward differences. The shear stress and heat flux terms appearing in M and N are backward differenced in the predictor step and forward differenced in the corrector step. When this method was applied to a two-dimensional, symmetric converging duct it was found that the symmetry of the flow field is better achieved by reversing the order of differencing for the predictor and corrector steps from one time-step to next time-step; i.e., if forward and backward differences are used in time-step n, then backward and forward differences should be used in time-step (n + 1). The order of differencing is also reversed for shear and heat flux terms. Details of the method and expressions for the predictor and corrector steps are given in reference 6.

A slightly modified form of the fourth order numerical damping, given in reference 8, is used in the present analysis to damp the oscillations which occur in the neighborhood of strong shocks in the flow field.

Boundary and Initial Conditions

The flow variables at the inflow boundary are free-stream values, whereas first order extrapolation is used to obtain the flow variables at the outflow boundary. For viscous flows, the following boundary conditions are applied along the surfaces:

BEST DOCUMENT AVAILABLE

$$\left.\begin{aligned} u &= 0 \\ v &= 0 \end{aligned}\right\} \text{(no-slip conditions)}$$

$$\frac{\partial T}{\partial n} = 0 \quad \text{(adiabatic wall)}$$

$$\frac{\partial p}{\partial n} = 0 \quad \text{(approximate boundary condition for } p\text{)}$$

where n is the normal to the surface.

For inviscid flows, the tangency condition is satisfied on the surfaces, i.e.,

$$\bar{v} = 0 \tag{7}$$

The above boundary conditions are applied in both the predictor and corrector steps. Initial conditions are normally prescribed for each set of calculations by assuming that free-stream conditions exist at all the grid points except at the boundaries where proper boundary conditions are applied.

RESULTS AND DISCUSSION

Calculations have been performed for two model inlet problems and two actual scramjet inlets having one and two struts, respectively. Detailed results for these cases are discussed in this section. All the results presented here are for air under a perfect gas assumption.

The first model problem is shown in figure 3(a). The inlet length is 10 cm with an initial height of 2 cm. The dimensions in this and the second

BEST DOCUMENT AVAILABLE

model problem have been fixed on the basis of certain features of the engine inlet flow, such as spillage, but are not typical of the actual engine dimensions. The top surface of the inlet produces a six-degree compression. The cowl plate is located in such a way that the shock wave from the top surface does not hit the cowl plate, thus leaving some space between the shock wave and the cowl plate to allow for flow spillage. A four-degree half-angle strut is placed in the flow as shown in the figure. The physical domain, in which the calculations are made, starts 1 cm ahead of the inlet, thus bringing the total length to 11 cm.

Figure 3(b) shows the inlet in the transformed plane. The boundary ABCD is transformed into a rectangular domain A'B'C'D', whereas the strut EFGH is transformed into a slit E'G'. Calculations are made for the following flow conditions at the inflow boundary of the inlet

$M_\infty = 5.0$

$P_\infty = 101{,}325\ N/m^2$ (1 atm)

$T_\infty = 293\ K$

Figure 4 and 5 show the pressure contours and velocity vector field, respectively, for the laminar flow. These plots are confined to the region downstream of line ZZ' in figure 3(a), where most of the flow distrubances take place. Upstream of line ZZ', the shock produced by the top surface turns the flow downward by about six degrees. Due to this, some of the flow spills out of the inlet just upstream of the cowl plate. The pressure contours in figure 4 clearly show the shocks and the expansion waves and their interactions with each other and with the inlet surfaces. The

BEST DOCUMENT AVAILABLE

velocity vector plot in figure 5 shows that the shock from the strut leading edge separates the boundary layer on the top surface of the inlet. A small separated region, caused by the shock from the cowl plate, is also produced near the trailing edge of the strut.

Figures 6(a) and 6(b) show the pressure distributions on the inlet top surface and strut upper and lower surfaces. The results in figure 6(a) are again plotted in the region downstream of line ZZ' in figure 3(a). The inviscid pressure distribution in figure 6(a) shows that the pressure on the top surface of the inlet remains constant downstream of the six-degree compression corner until the shock from the leading edge of the strut upper surface hits the top surface and is reflected. This produces a large pressure increase on the top surface. The expansion waves from the strut shoulder interact with the leading edge shock and with the top surface. This results in a gradual decrease in the pressure on the top surface. Figure 6(b) shows that the pressure on the strut upper surface increases due to the leading edge shock. The pressure remains constant until the expansion waves at the strut shoulder decrease it. The flow goes through a small expansion again near the trailing edge of the strut. The pressure distribution on the lower surface of the strut shows that the flow undergoes two expansions produced by the strut leading edge and shoulder. The pressure increases near the trailing edge due to the shock from the cowl plate.

The pressure distributions for the laminar flow are similar to those for the inviscid flow with two differences. First, the pressure level is slightly higher for the viscous flow due to the increase in effective compression angle. Second, the induced shock due to the boundary-layer

BEST DOCUMENT AVAILABLE

separation causes an increase in the pressure as seen in figure 6(a) around x = 8.5 cm.

As mentioned earlier, the geometry of the problem is such that the inlet does not capture the entire mass entering it. Some mass is spilled from the lower boundary ahead of the cowl plate. The present inviscid code predicts a flow spillage of 2.64 kg/s, which is in excellent agreement with the value of 2.65 kg/s as calculated from the exact shock theory. For the laminar flow, the spillage is expected to increase due to steeper shock. The present code predicts 3.74 kg/s spillage for the laminar flow. The exact inviscid flow spillage for a 6.5° compression angle is 3.71 kg/s. This shows that the effective change in the body compression angle due to viscous effects in the laminar flow is approximately 0.5°.

The geometry of the second model inlet problem is shown in figure 7. The inlet length is 10 cm with an initial height of 1.5 cm. The calculations are made in the region starting 1 cm ahead of the inlet, thus bringing the total length to 11 cm. The top surface produces a 10° compression at x = 1 cm and then a 20° expansion at x = 6 cm. The cowl plate is again located in such a way that the shock from the top surface does not hit it, thus allowing a fraction of the flow to spill out of the inlet. The flow conditions at the inflow boundary of the inlet are taken to be the same as in the previous problem. Calculations are made for inviscid, laminar, and turbulent flows.

Figures 8 and 9 show the velocity vector field and pressure contours, respectively. For clarity, these plots are shown in the region downstream of the expansion corner from x = 6 cm to the end of the inlet. Upstream of

BEST DOCUMENT AVAILABLE

the expansion corner, the shock from the top surface turns the flow downward by about 10°. Due to this, some flow spills out of the inlet ahead of the cowl plate. The velocity vector fields in figure 8 are plotted for the laminar and turbulent flows only. It is seen that the laminar boundary layer on the top surface separates due to the interaction of the cowl plate shock with the boundary layer on the top surface. The separation completely disappears for the turbulent flow under present flow conditions, since the turbulent boundary layer is able to accept higher adverse flow gradients without separating.

The pressure contours in figure 9 are shown for inviscid, laminar, and turbulent flows. These contour plots clearly show the interaction of the cowl plate shock with the expansion waves from the top surface. Due to this interaction, the shock hits the top surface earlier than it would have without the interaction. The expansion waves go through the shock and attenuate the pressure on the cowl plate, whereas the shock is reflected from the top surface. It is also seen that the cowl plate shock hits the top surface far downstream for the inviscid flow, as compared to the laminar and turbulent flows. This is directly due to the viscous effects which make the shock steeper due to the increased effective body angle.

Figure 10 shows the pressure distribution on the top surface for the inviscid and laminar flows. The pressure is seen to increase due to the compression at x = 1 cm. It remains constant until it is decreased due to the expansion at x = 6 cm. It again remains constant until the cowl plate shock hits the top surface, which increases the pressure. The gradual decrease in the surface pressure towards the end of the inlet is due to the expansion waves which hit the top surface after being reflected from the

BEST DOCUMENT AVAILABLE

cowl plate. As expected, the pressure level for the laminar flow is seen to be slightly higher than that for the inviscid flow due to viscous effects. Although not shown here, the pressure level for the turbulent flow was even higher than that for the laminar flow.

The flow which spills from the lower boundary, as calculated by the present analysis, is 9.26 kg/s for the inviscid flow, 11.26 kg/s for the laminar flow, and 13.41 kg/s for the turbulent flow. The exact values for the inviscid flow are 9.76 kg/s for 10° compression, 11.38 kg/s for 10.5° compression and 13.10 kg/s for 11° compression. Thus, this problem also shows that the effective change in the body compression angle due to viscous effects is approximately 0.5° for the laminar flow and 1° for the turbulent flow.

In the next two problems, the flow field in a more practical scramjet inlet configuration having one or two struts is analyzed using the two-dimensional code. Before discussing the results for these problems, a brief description is given to explain how the two-dimensional analysis may be used to approximately calculate certain features of a three-dimensional inlet of the type shown in figure 2.

Figure 11 shows the side view of a scramjet module. The sidewall leading edges are swept back at an angle ω, and the Mach number at the face of the inlet is M_1. If the shock waves in the inlet do not detach and if the end effects are neglected, the component of the velocity parallel to sidewall sweep should remain unchanged, and the flow disturbances should occur in the plane ZZ' normal to the sidewall leading edge. The flow can therefore be solved using the two-dimensional code in the plane ZZ'

BEST DOCUMENT AVAILABLE

with Mach number M_{1N}. The solution in the ZZ' plane can be projected to the plane of the cowl, and the velocity distribution in the plane of the cowl can be obtained by superimposing the constant velocity component over the above solution. Knowing the velocity and density distributions, it is possible to calculate the flow spillage from the three-dimensional inlet as a function of cowl location. Thus, the two-dimensional analysis may be used in preliminary studies of the effects of strut and cowl locations and their shapes on inlet spillage. The two-dimensional analysis can also give an indication as to whether or not the inlet will start for a given set of flight conditions.

The analysis for one-and two-strut inlets has been carried out in the plane ZZ'. The sidewall leading edge sweep is prescribed as 33°. Realistic flow conditions are used in the analysis and are tabulated in table 1. The one-strut inlet is discussed first. Its geometry is shown in figure 12; the initial width of the inlet is 15 cm, and other dimensions and angles are shown in the figure. Figure 13 shows the pressure contours for the inviscid flow at three Mach numbers. No solution could be obtained at the lowest Mach number, $M_\infty = 4$, for which the shock waves detached in the inlet. For this case, after a sufficient number of time-steps, a normal shock formed just downstream of the inflow boundary, resulting in a large mass imbalance. The mass imbalance occurs when the governing equations fail to produce a solution for the prescribed inflow boundary conditions, i.e., the inlet minimum area section cannot pass the inflow mass and the flow chokes. It is seen from the contour plots in figure 13 that the shock wave from the sidewall coalesces with the shock wave from the strut leading edge to form a stronger shock. For the laminar flow, the strong shock, formed by the shock

BEST DOCUMENT AVAILABLE

wave coalescence, caused a large separated region on the sidewall, which produced an induced shock in front of the separated region. The induced shock choked the flow in a manner similar to that described earlier, and again no meaningful solution could be obtained at any of the Mach numbers considered here. For the turbulent flow, the solution could be obtained at the highest Mach number but the flow choked again at lower Mach numbers. Table 2 summarizes the conditions for which the solutions could or could not be obtained. These are represented in the table by start and unstart of the inlet, respectively.

To eliminate the problem of shock wave coalescence, a two-strut inlet is considered. The geometry of this inlet is shown in figure 14. The initial width of the inlet is again 15 cm. Other dimensions and angles are shown in the figure. The strut surface, on which the shock from the sidewall strikes, is kept parallel to the oncoming flow so that no shock is produced by this surface. This avoids the possibility of shock wave coalescence. Figure 15 shows the pressure contours for the laminar flow at three Mach numbers. The corresponding velocity vector fields are shown in figure 16. No viscous flow solution could be obtained for the lowest Mach number due to the choking of the flow caused by the boundary-layer separation. The solutions could be obtained at all Mach numbers for the inviscid flow. Table 3 summarizes the conditions for which the solutions could or could not be obtained. The table clearly shows the improvement in the performance of the two-strut inlet over the one-strut inlet.

The computations for all of the preceding problems were made on a CDC-Cyber-203 vector processing computer (an upgraded version of CDC-STAR-100

BEST DOCUMENT AVAILABLE

computer) using a mesh size of 51 × 51. The solution marches about 20 time-steps per second for the viscous flow and about 30 time-steps per second for the inviscid flow. A typical solution is obtained in two to five minutes depending upon the number of time-steps required for convergence.

CONCLUSIONS

Two-dimensional Navier-Stokes equations have been used to analyze the scramjet inlet flow. The analysis uses a numerical coordinate transformation which generates a set of boundary-fitted curvilinear coordinates. The embedded bodies in the flow field are transformed into slits. MacCormack's time-dependent, finite-difference method is used to solve the governing equations. A two-layer eddy viscosity model is used for the turbulent flow. The code can analyze both inviscid and viscous flows with no-strut, one-strut, or multiple struts in the flow field.

Results are presented for two model problems and two actual scramjet inlets. The code predicts the complex wave interactions and shock-boundary layer interactions very well. The application of the two-dimensional analysis in preliminary design studies of the scramjet inlet is briefly discussed. It is shown that the two-dimensional analysis can also give an indication as to whether or not the inlet will aerodynamically choke for a given set of flight conditions. An extension of the code to analyze full three-dimensional inlets is currently underway.

BEST DOCUMENT AVAILABLE

REFERENCES

1. Jones, R. A.; and Huber, P. W.: Toward Scramjet Aircraft, Astronautics and Aeronautics, Vol. 16, No. 2, Feb. 1978, pp. 38-49.

2. Beach, H. L., Jr.: Hypersonic Propulsion. Paper No. XII Aeropropulsion, NASA CP-2092, 1979.

3. Trexler, C. A.: Design and Performance at a Local Mach Number of 6 of an Inlet for an Integrated Scramjet Concept. NASA TN D-7944, 1975.

4. Anderson, G. Y.: Hypersonic Propulsion. Paper No. VI Aeronautical Propulsion, NASA SP-381, 1975.

5. Thompson, J. F.; Thames, F. C.; and Mastin, C. W.: Boundary-Fitted Curvilinear Coordinate Systems for Solution of Partial Differential Equations on Fields Containing Any Number of Arbitrary Two-Dimensional Bodies. NASA CR-2729, 1977.

6. MacCormack, R. W.: The Effect of Viscosity in Hypervelocity Impact Cratering. AIAA Paper No. 69-354, 1969.

7. Baldwin, B. S.; and Lomax, H.: Thin Layer Approximation and Algebraic Model for Separated Turbulent Flows. AIAA Paper No. 78-257, 1978.

8. Drummond, J. P.: Numerical Investigation of the Perpendicular Injector Flow Field in a Hydrogen Fueled Scramjet. AIAA Paper No. 79-1482, 1979.

BEST DOCUMENT AVAILABLE

Table 1. Flow conditions.

M_∞	M_1	M_{1N}	P_1 (atm)	T_1 (°K)
4	3.43	2.88	0.095	322
5	4.29	3.60	0.064	328
6	5.18	4.34	0.045	329
7	6.00	5.032	0.035	335

BEST DOCUMENT AVAILABLE

Table 2. Solution conditions for one-strut inlet.

Mach Number (M_∞)	Type of Flow		
	Inviscid	Laminar	Turbulent
7	Start	Unstart	Start
6	Start	Unstart	Unstart
5	Start	Unstart	Unstart
4	Unstart	Unstart	Unstart

BEST DOCUMENT AVAILABLE

Table 3. Solution conditions for two-strut inlet.

Mach Number (M_∞)	Type of Flow		
	Inviscid	Laminar	Turbulent
7	Start	Start	Start
6	Start	Start	Start
5	Start	Start	Start
4	Start	Unstart	Unstart

BEST DOCUMENT AVAILABLE

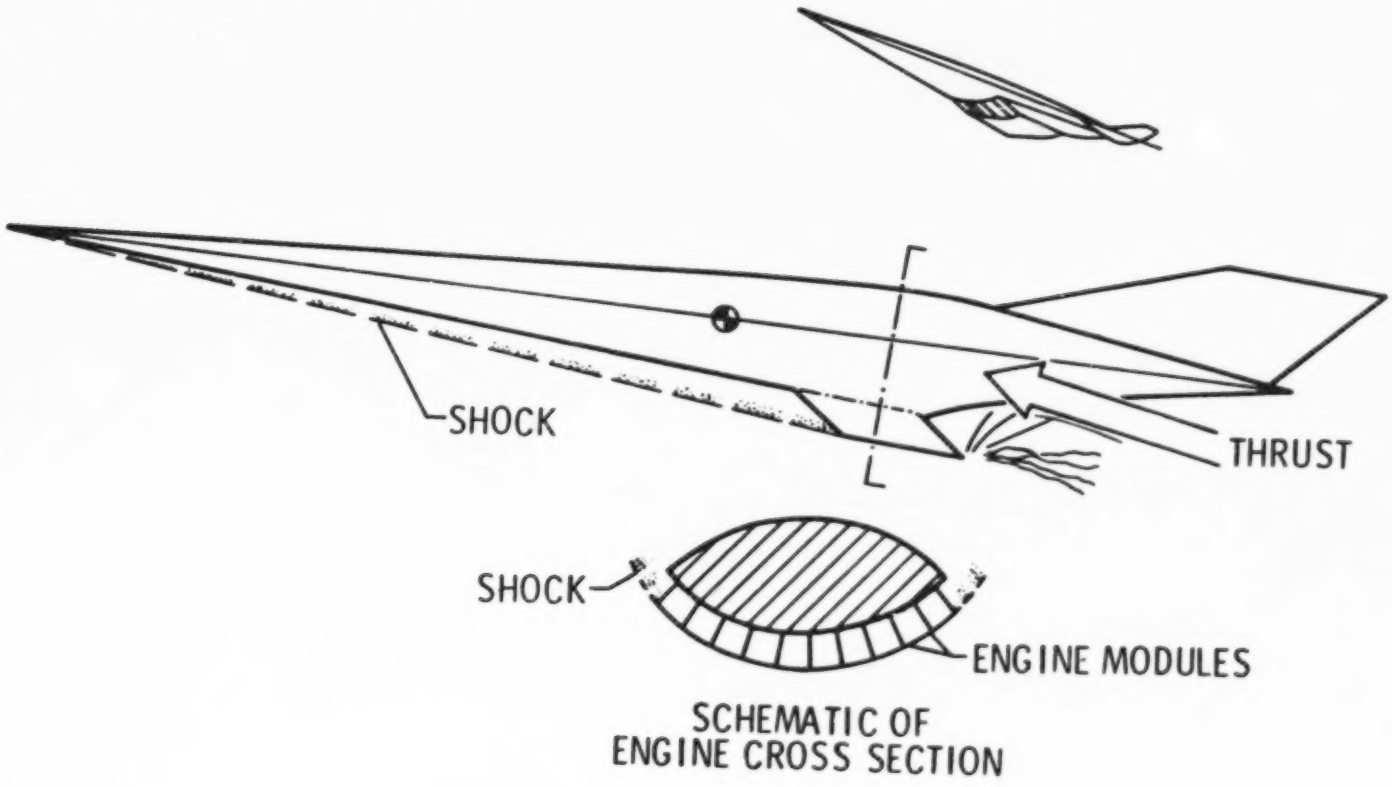

Figure 1. Airframe-integrated scramjet engine concept.

BEST DOCUMENT AVAILABLE

BEST DOCUMENT AVAILABLE

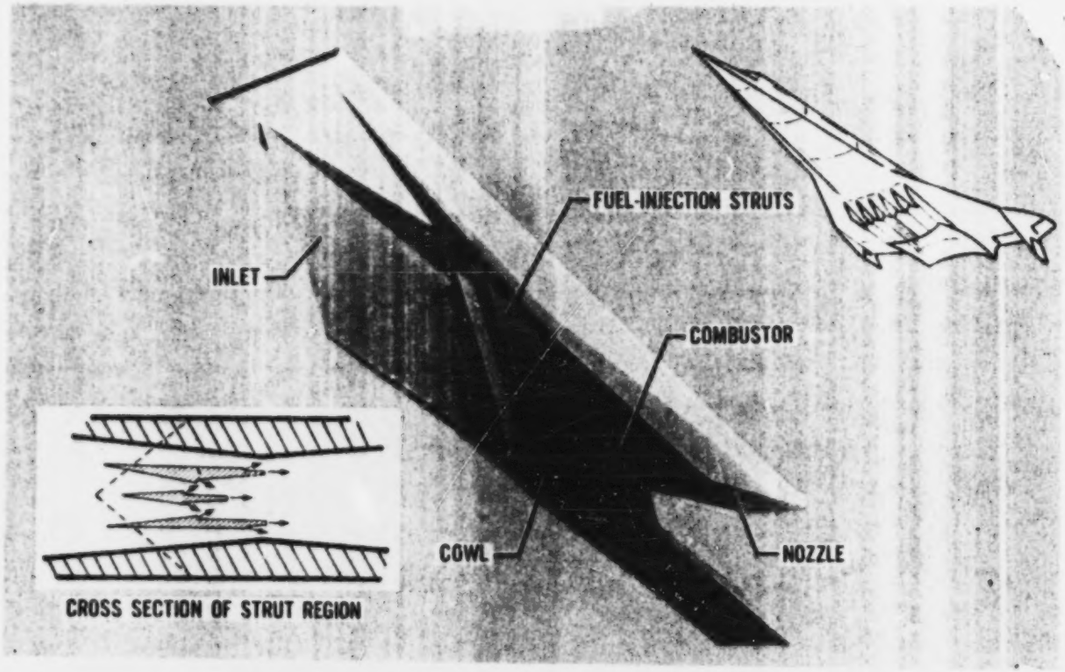

Figure 2. Scramjet engine module and its cross section.

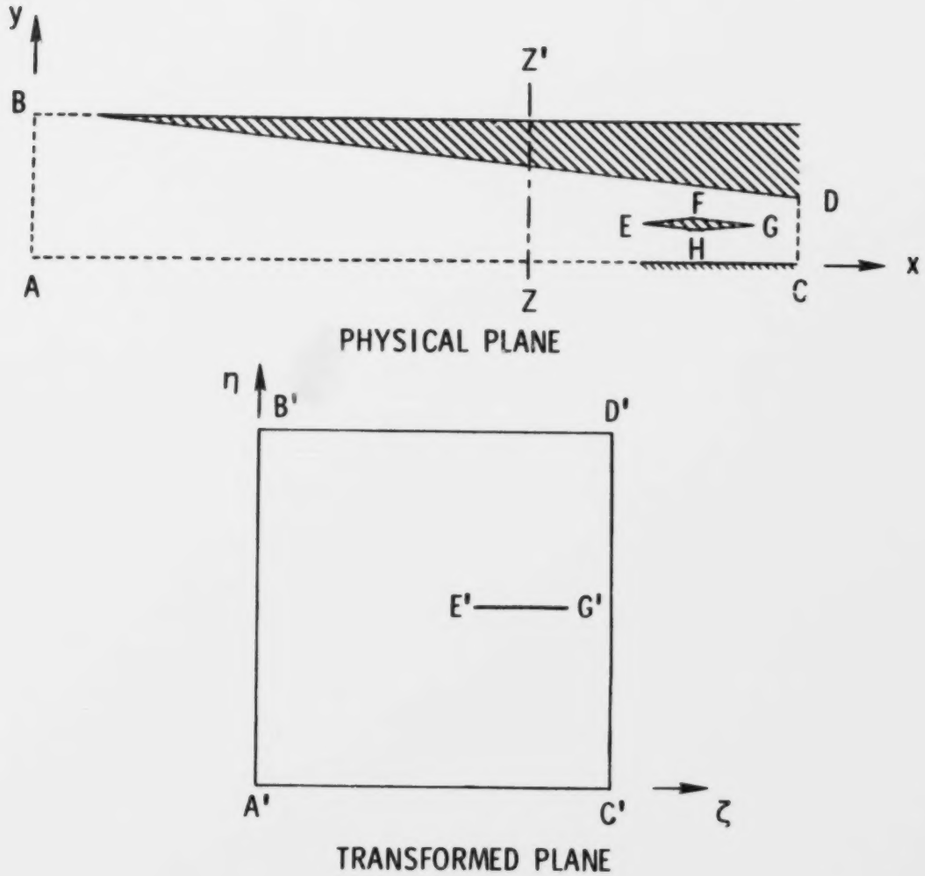

Figure 3. Geometry of the first model problem.

BEST DOCUMENT AVAILABLE

BEST DOCUMENT AVAILABLE

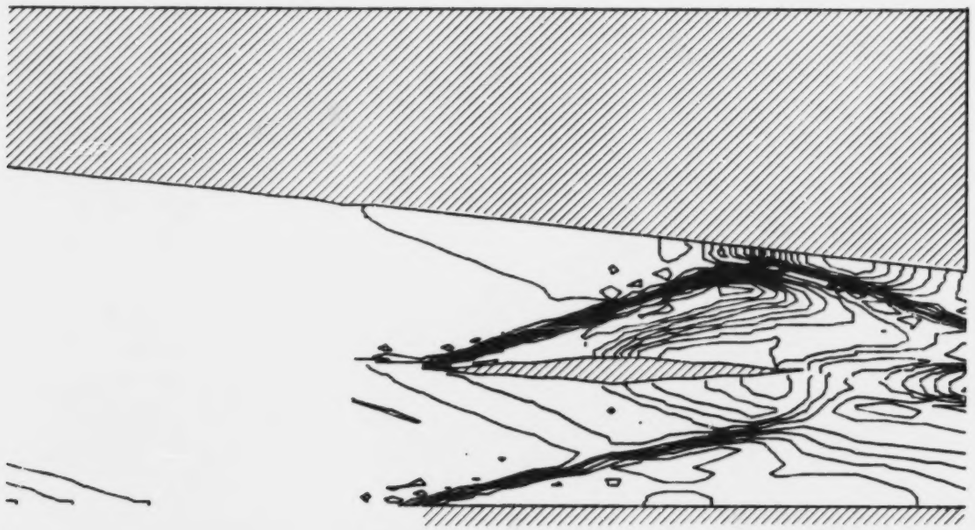

Figure 4. Pressure contours downstream of line ZZ'.

VELOCITY VECTOR FIELD DOWNSTREAM OF LINE ZZ'

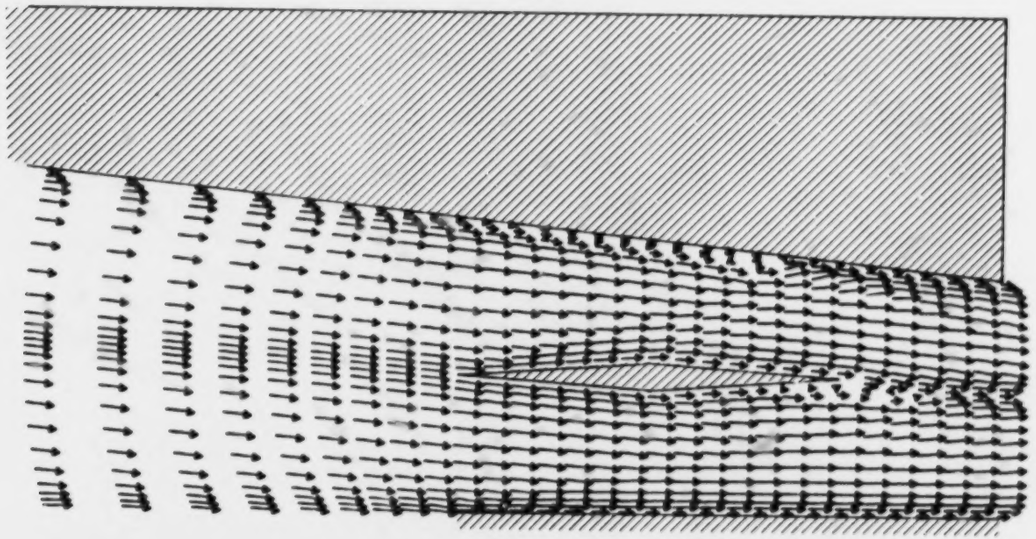

Figure 5. Velocity vector field downstream of line ZZ'.

BEST DOCUMENT AVAILABLE

BEST DOCUMENT AVAILABLE

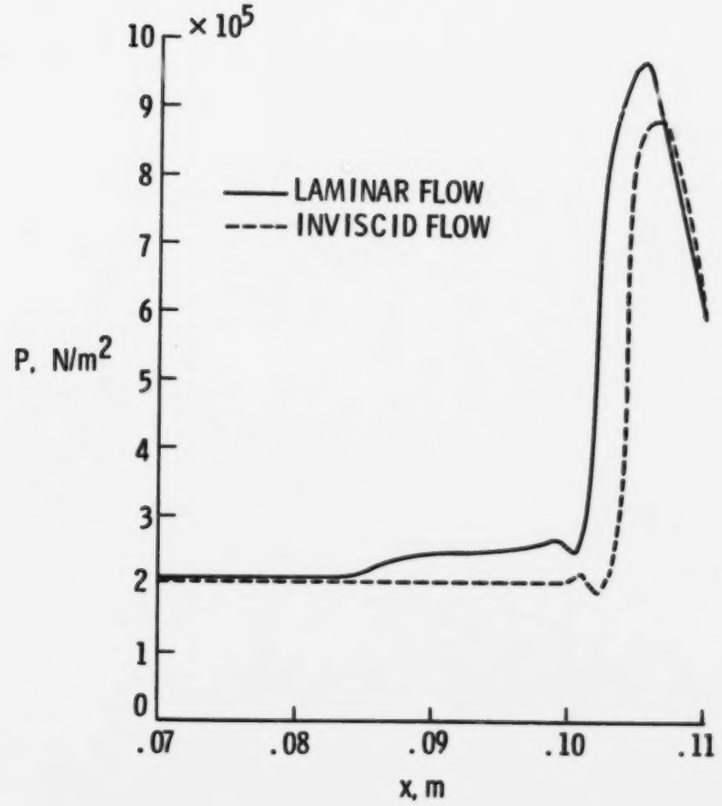

Figure 6(a). Pressure distribution on the top surface of the inlet downstream of line ZZ'.

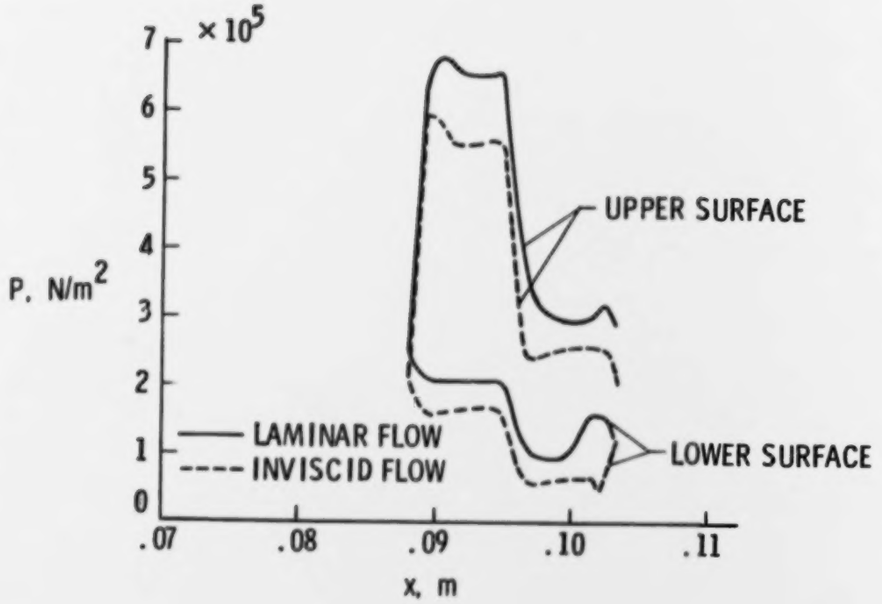

Figure 6(b). Pressure distribution around the strut.

BEST DOCUMENT AVAILABLE

BEST DOCUMENT AVAILABLE

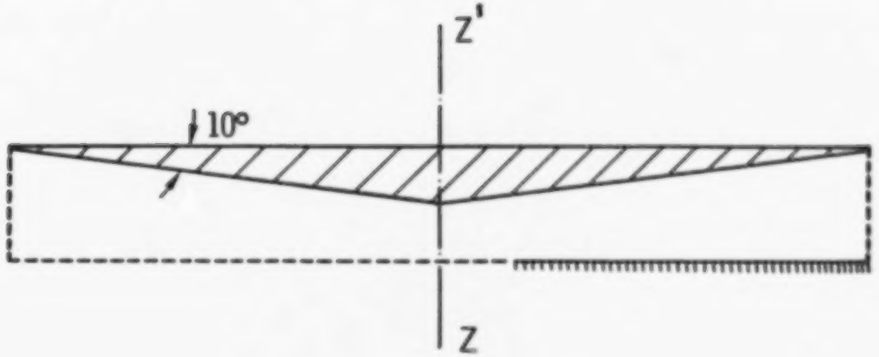

Figure 7. Geometry of the second model problem.

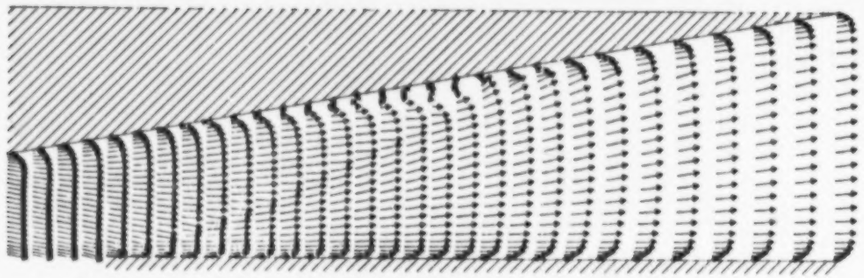

Figure 8. Velocity vector field downstream of line ZZ'.

BEST DOCUMENT AVAILABLE

BEST DOCUMENT AVAILABLE

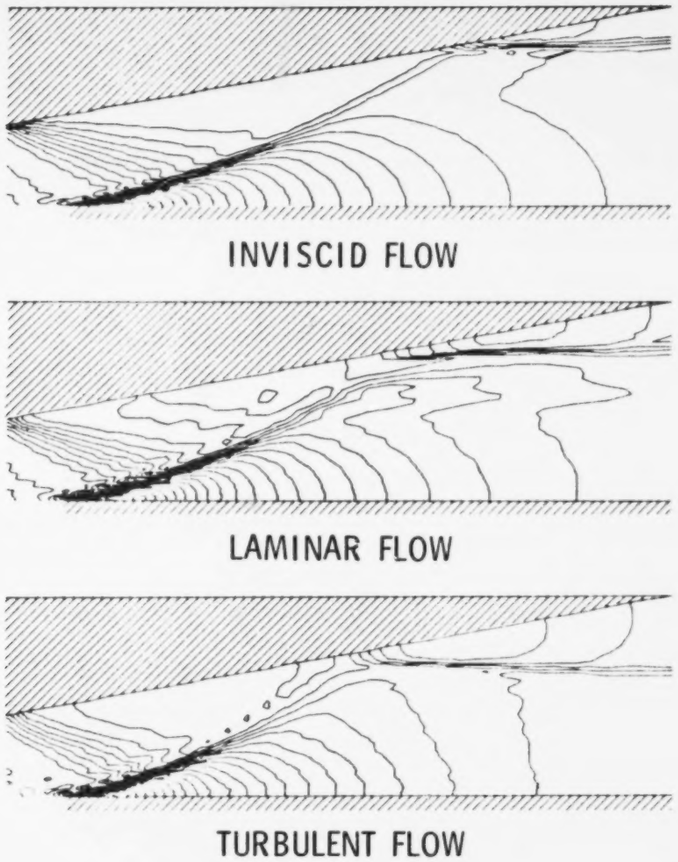

Figure 9. Pressure contours downstream of line ZZ'.

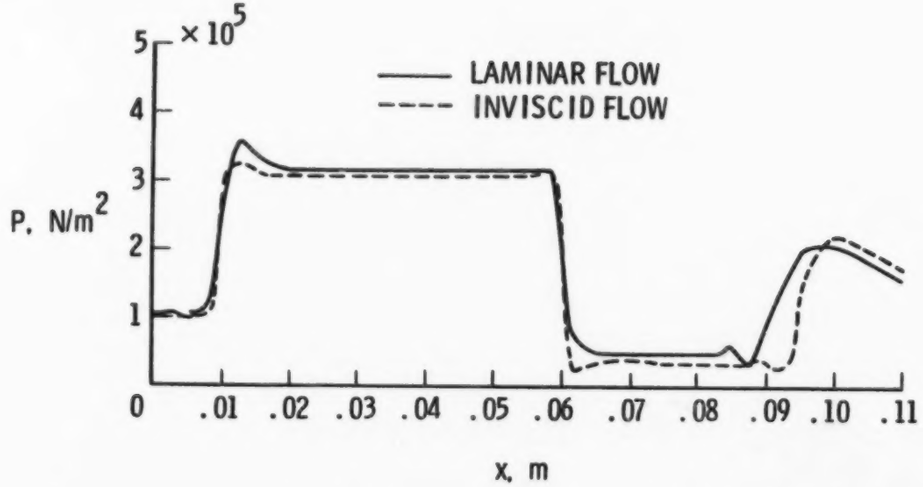

Figure 10. Pressure distribution on the top surface of the inlet.

BEST DOCUMENT AVAILABLE

BEST DOCUMENT AVAILABLE

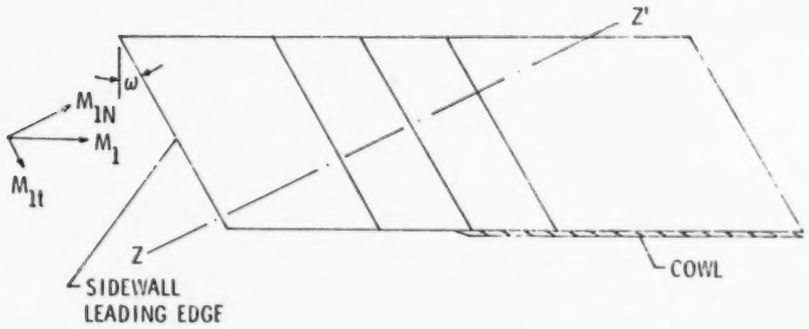

Figure 11. Side view of a scramjet module.

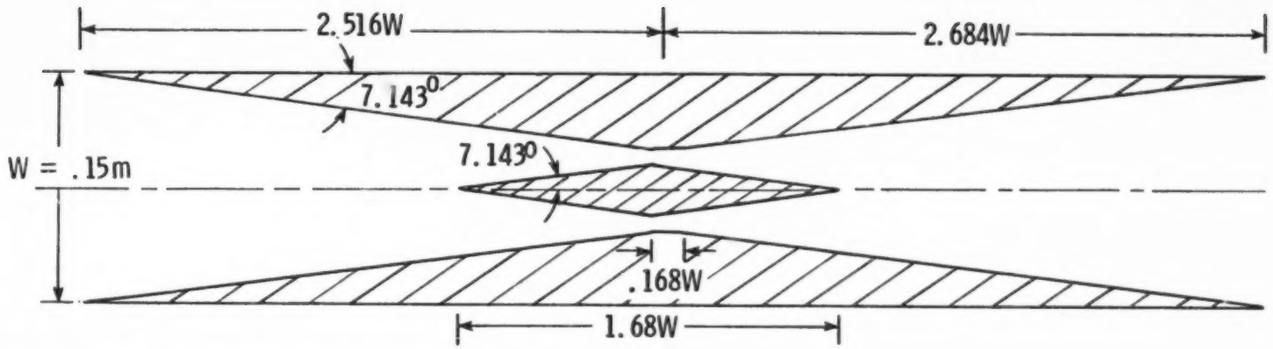

Figure 12. Geometry of one-strut inlet in a plane normal to sidewall leading edge.

BEST DOCUMENT AVAILABLE

BEST DOCUMENT AVAILABLE

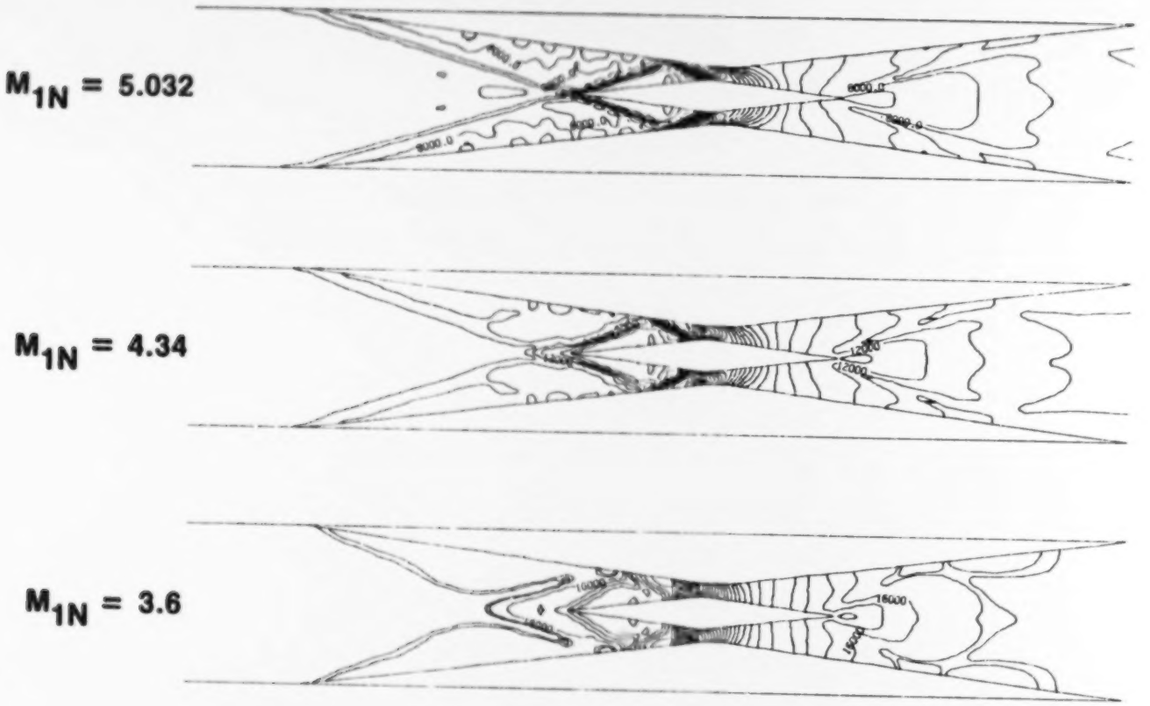

Figure 13. Pressure contours for inviscid flow at various Mach numbers.

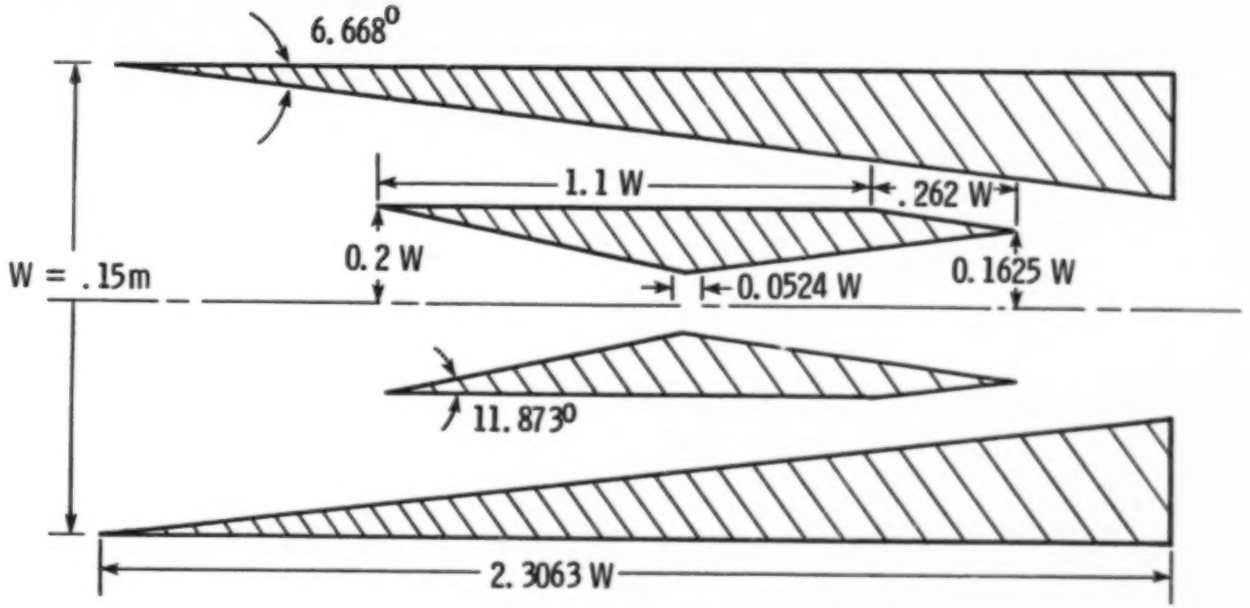

Figure 14. Geometry of two-strut inlet in a plane normal to sidewall leading edge.

BEST DOCUMENT AVAILABLE

BEST DOCUMENT AVAILABLE

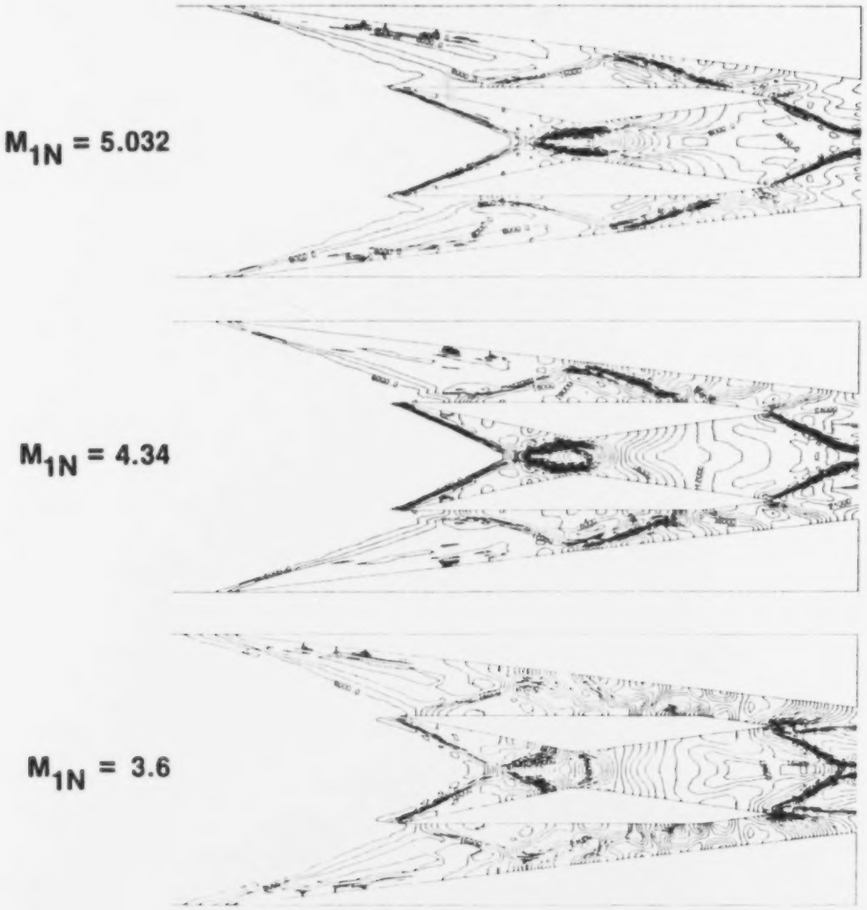

Figure 15. Pressure contours for laminar flow at various Mach numbers.

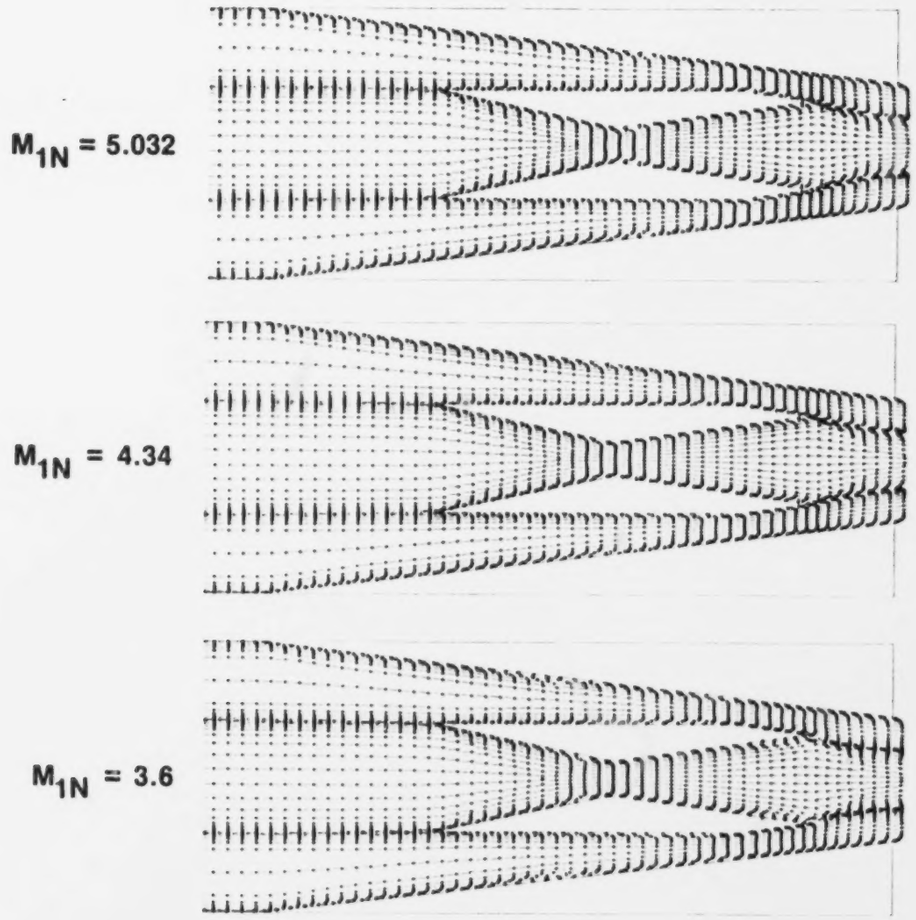

Figure 16. Velocity vector field for laminar flow at various Mach numbers.

BEST DOCUMENT AVAILABLE

BEST DOCUMENT AVAILABLE

1. Report No.	2. Government Accession No.	3. Recipient's Catalog No.
NASA CR-3562		

4. Title and Subtitle	5. Report Date
ANALYSIS OF THE SCRAMJET INLET FLOW FIELD USING TWO-DIMENSIONAL NAVIER-STOKES EQUATIONS	June 1982
	6. Performing Organization Code

7. Author(s)	8. Performing Organization Report No.
Ajay Kumar and S.N. Tiwari	
	10. Work Unit No.

9. Performing Organization Name and Address	11. Contract or Grant No.
Old Dominion University Research Foundation P.O. Box 6369 Norfolk, Virginia 23508-0369	NAS1-15930
	13. Type of Report and Period Covered Contractor Report 11/1/79-10/31/81

12. Sponsoring Agency Name and Address	14. Sponsoring Agency Code
National Aeronautics and Space Administration Washington, DC 20546	

15. Supplementary Notes

Langley Technical Monitor: J. Philip Drummond

Final Report

Ajay Kumar was formerly employed by Old Dominion University

16. Abstract

A computer code has been developed to solve the full two-dimensional Navier-Stokes equations in a scramjet inlet. The analysis uses a numerical coordinate transformation which generates a set of boundary-fitted curvilinear coordinates. The explicit finite-difference algorithm of MacCormack is used to solve the governing equations. A two-layer eddy viscosity model is used for the turbulent flow. The code can analyze both inviscid and viscous flows with multiple struts in the flow field. Detailed results are presented for two model problems and two scramjet inlets with one and two struts. The application of the two-dimensional analysis in the preliminary design of the actual scramjet inlet is briefly discussed.

17. Key Words (Suggested by Author(s))	18. Distribution Statement
Scramjet Inlet Flow	Unlimited - Unclassified Subject Category 34

19. Security Classif. (of this report)	20. Security Classif. (of this page)	21. No. of Pages	22. Price*
Unclassified	Unclassified	44	A03

* For sale by the National Technical Information Service, Springfield, Virginia 22161

NASA-Langley, 1982